

Swinburne Research Bank

<http://researchbank.swinburne.edu.au>



Fasano, G., et al. (2010). The shapes of BCGs and normal ellipticals in nearby clusters.

Originally published in *Monthly Notices of the Royal Astronomical Society*, 404(3), 1490–1504.

Available from: <http://dx.doi.org/10.1111/j.1365-2966.2010.16361.x>

Copyright © 2010 The authors.

This is the author's version of the work, posted here with the permission of the publisher for your personal use. No further distribution is permitted. You may also be able to access the published version from your library. The definitive version is available at www.interscience.wiley.com.

The Shapes of BCGs and normal Ellipticals in Nearby Clusters

G. Fasano^{1*}, D. Bettoni¹, B. Ascaso^{2,5}, G. Tormen³, B.M. Poggianti¹, T. Valentini³, M. D’Onofrio³, J. Fritz¹, A. Moretti¹, A. Omizzolo^{1,9}, A. Cava^{4,1}, M. Moles^{5,10}, A. Dressler⁶, W.J. Couch⁷, P. Kjærgaard⁸ and J. Varela¹.

¹*INAF, Osservatorio Astronomico di Padova, Vicolo Osservatorio 5, 35122 Padova, Italy*

²*Dept. of Physics, University of California, Davis, One Shields Avenue, CA 95616, USA*

³*Dip. Astronomia, Università di Padova, Vicolo dell’Osservatorio 2, 35122 Padova, Italy*

⁴*Instituto de Astrofísica de Canarias La Laguna, Spain*

⁵*Instituto de Astrofísica de Andalucía, Camino Bajo de Hueter 50, 18008 Granada, Spain*

⁶*The Observatories of the Carnegie Institution of Washington, Pasadena, USA*

⁷*Center for Astrophysics, Swinburne University of Technology, Australia*

⁸*Copenhagen University Observatory, Niels Bohr Institute for Astronomy, Denmark*

⁹*Specola Vaticana, 00120 Stato Città del Vaticano*

¹⁰*Centro de Estudios de Física del Cosmos de Aragón(CEFCA), C/General Pizarro, 1, 44001 Teruel, Spain*

Accepted Received; in original form

ABSTRACT

We compare the apparent axial ratio distributions of Brightest Cluster Galaxies (BCGs) and normal ellipticals (Es) in our sample of 75 galaxy clusters from the WINGS survey. Most BCGs in our clusters (69%) are classified as cD galaxies. The sample of cDs has been completed by 14 additional cDs (non-BCGs) we found in our clusters. We deproject the apparent axial ratio distributions of Es, BCGs and cDs using a bi-variate version of the rectification Lucy’s algorithm, whose results are supported by an independent Monte-Carlo technique. Finally, we compare the intrinsic shape distribution of BCGs to the corresponding shape distribution of the central part of cluster-sized dark-matter halos extracted from the GIF2 Λ CDM N -body simulations.

We find that: (i) Es have triaxial shape, the triaxiality sharing almost evenly the intrinsic axial ratios parameter space, with a weak preference for prolateness; (ii) the BCGs have triaxial shape as well. However, their tendency towards prolateness is much stronger than in the case of Es. Such a strong prolateness appears entirely due to the sizeable (dominant) component of cDs inside the WINGS sample of BCGs. In fact, while the ‘normal’ (non-cD) BCGs do not differ from Es, as far as the shape distribution is concerned, the axial ratio distribution of BCG_cD galaxies is found to support quite prolate shapes; (iii) our result turns out to be strongly at variance with the only similar, previous analysis by Ryden et al. (1993, RLP93), where BCGs and Es were found to share the same axial ratio distribution; (iv) our data suggest that the above discrepancy is mainly caused by the different criteria that RLP93 and ourselves use to select the cluster samples, coupled with a preference of cDs to reside in powerful X-ray emitting clusters; (v) the GIF2 N -body results suggest that the prolateness of the BCGs (in particular the cDs) could reflect the shape of the associated dark matter halos.

Key words: galaxies: clusters – galaxies:general – galaxies: elliptical and lenticular – galaxies:cD

1 INTRODUCTION

Rich galaxy clusters show in their central part a remarkable concentration of galaxies, surrounded by progressively

* E-mail: giovanni.fasano@oapd.inaf.it

less dense regions. The brightest cluster galaxies (BCGs) are usually elliptical-like galaxies, often much brighter than the rest of the global population of Es (Sandage and Hardy 1973; Schombert 1986, 1992). They are normally found close to the peaks of galaxy number density (Beers and Geller 1983) and X-ray emission (Jones and Forman 1984) of the cluster. The significant alignment between the elongations of the BCGs and their host clusters in both the optical (Carter and Metcalfe 1980; Struble 1990; Plionis et al. 2003) and X-ray bands (Hashimoto et al. 2008), together with the correlations between BCGs luminosity and cluster properties (i.e. X-ray temperature; Edge and Stewart 1991), suggests that the formation history of BCGs is closely linked to that of the host clusters (Kormendy and Djorgovski 1989; Coziol et al. 2009).

Among the different formation scenarios which have been proposed in the literature for BCGs, we mention: (i) merging of compact galaxy groups before or during cluster assembly and virialization (Ostriker and Tremaine 1975; White 1976; Merritt 1985, see also N -body simulations by Dubinski 1998); (ii) filament driven, regular accretion of small, gas-rich proto-galactic units (West 1994); (iii) tidal stripping from other cluster galaxies (Gallagher and Ostriker 1972; Richstone 1975, 1976); (iv) continuous accretion of star forming gas from the intra-cluster medium (cooling flows; Silk 1976; Fabian 1994); (v) late assembling ($z \sim 0.5$) of smaller, gas-poor (red) galaxies in hierarchical scenario (De Lucia and Blaizot 2007; Bernardi et al. 2007). Although each one of the proposed mechanisms turns out to present some drawbacks when compared with the observations, all of them are likely to contribute, with different strength and timings, to the whole process of formation of BCGs.

From the observational point of view, the BCGs are special in many aspects: besides the unusually high luminosity, the BCGs exhibit huge sizes, sometimes further enlarged by diffuse, very extended halos. In this case they are called cD galaxies and their sizes may even reach ~ 300 kpc (Oemler 1976; Schombert 1988). The BCGs are also extremely massive objects (up to $\sim 10^{13} M_{\odot}$), with peculiar kinematics, in that they have lower velocity dispersions and larger radii than predicted by the Faber-Jackson and Kormendy relations (Thuan and Romanishin 1981; Hoessel et al. 1987; Schombert 1987; Oegerle and Hoessel 1991; Bernardi et al. 2007), consistent with the presence of a larger fraction of dark matter (von der Linden et al. 2007) and/or with significant growth of BCGs via dissipationless mergers (Desroches et al. 2007). Finally, the BCGs often display multiple nuclei (Schneider et al. 1983; Laine et al. 2003) and have been frequently identified as powerful radio sources (Giacintucci et al. 2007).

The fact that BCGs are peculiar in so many aspects with respect to the population of normal Es, might suggest that their shape too differs from that of Es. Also, the special role played by BCGs in the formation history of clusters could result in a rather peculiar shape. Normal ellipticals are generally believed to cover the whole range of triaxiality (Fasano and Vio 1991; Ryden 1992; Bak and Statler 2000), while both evolutionary scenarios supported by simple dynamical considerations (West 1994) and N -body simulations of self-consistent models of galaxy clusters including dark matter component (Dubinski 1998), both predict BCGs

with significantly prolate shapes. Remarkably enough, also the N -body simulations of BCGs-scale, dark-matter halos in Λ CDM cosmology lead to similar conclusions about their shape (Warren et al. 1992; Bailin and Steinmetz 2005; Allgood et al 2006; Bett et al. 2007), with the additional, interesting hint that the dark matter halos become more prolate towards their inner part and at increasing the halo mass (Cole and Lacey 1996; Gottlöber and Yepes 2007). In spite of these converging indications, the only direct comparison available up to now in the literature between the observed axial ratio distributions of BCGs and Es (Ryden et al. 1993, hereafter RLP93, observations in the Kron-Cousins R band) led to the conclusion that they are very similar.

In this paper we perform a new comparison between the distributions of the observed axial ratios (hereafter $q = \text{minor-axis} / \text{major-axis}$) of BCGs and Es exploiting the large database of nearby cluster galaxies provided by the WINGS survey (Fasano et al. 2006; Varela et al. 2009). We pay particular attention to the distinction between normal BCGs and cDs, thus including in the sample the non-BCGs, cD galaxies. We also deproject the apparent axial ratio distributions to get the corresponding distributions of the intrinsic axial ratios. Finally, using the GIF2 Λ CDM cosmological simulations, we extract 3510 cluster-sized dark-matter halos and calculate the central shape at the corresponding BCG scale, allowing us to compare their intrinsic axial ratio distributions with those of the observed BCGs.

In Section 2 we describe the galaxy sample and the axial ratio data we use in our analysis. In Section 3 the axial ratio distributions of Es, BCGs and cDs are presented and discussed and the comparison with the results of RLP93 is performed. Section 4 outlines the technical aspects of the deprojection and presents the distributions of the intrinsic axial ratios we obtain applying such deprojection techniques to the Es, BCGs and cDs samples. In Section 5 we discuss our results and compare the intrinsic shapes of BCGs to those obtained from the GIF2 N -body data. Finally, Section 6 summarize our conclusions. Throughout the paper we use the following cosmology: $H_0 = 70 \text{ kms}^{-1} \text{ Mpc}^{-1}$, $\Omega_M = 0.3$ and $\Omega_{\Lambda} = 0.7$.

2 GALAXY SAMPLES AND AXIAL RATIO DATA

We have extracted our samples of BCGs and Es from the Wide-field Nearby Galaxy-cluster Survey (WINGS; Fasano et al. 2006). The 77 clusters of the WINGS sample were selected, in the redshift range 0.04-0.07, from ROSAT catalogs of clusters (Ebeling et al. 1996, 1998, 2000) and turn out to cover a wide range of masses ($\sim 5 \times 10^{13} - 3.2 \times 10^{15} M_{\odot}$; $\text{Log} L_X \sim 43.3 - 44.7 \text{ ergs s}^{-1}$). The optical WINGS survey provides B- and V-band imaging of the whole sample of clusters. Integrated and aperture photometry have been obtained for $\sim 400,000$ galaxies by using SExtractor (Bertin and Arnouts 1996). The procedures adopted to avoid mutual photometric contamination between big galaxies with extended halos and smaller, halo-embedded companions are described in detail in Varela et al. (2009). We just recall here that the largest galaxies in each cluster were carefully modeled with IRAF-ELLIPSE and removed from the original images in order to allow a reliable

masking of the small companions when performing the surface photometry of the big galaxies themselves. The BCG in Abell 3164 has been excluded from the sample since its surface photometry turned out to be uncertain due to the proximity of the inter-chip region of the CCD mosaic, while the BCG in Abell 3562 was not included due to the quality of the WINGS imaging for this cluster is not good enough to allow a reliable surface photometry and morphology estimate. Thus, the final sample of BCGs consists of 75 galaxies.

We have classified their morphology using the WINGS V-band imaging (Fasano et al. 2006) and the purposely devised, automatic tool MORPHOT (Fasano et al. 2010, in preparation; see also Fasano et al. 2007; Poggianti et al. 2009; Valentinuzzi et al. 2009). The logical sequence and the basic procedures of MORPHOT are outlined in the Appendix, with particular reference to its capability of disentangling cDs from BCG_Es.

On the other hand, the quantitative, multi-component analysis of the luminosity profiles has been performed, on both the V- and B-band WINGS images, using GASP2D (Ascaso et al. 2010, in preparation; see also Méndez-Abreu et al. 2008). In this case, cD galaxies have been identified by the simultaneous occurrence of two conditions: (i) the presence, in the outer profiles, of a light excess (with respect to the inner Sersic component) significantly larger than the photometric errors; (ii) the positioning around a surface brightness level of $\mu_V \sim 24$ of the ‘breaking point’ where the profile splits up from the inner profile. When MORPHOT and GASP2D (in both V- and B-band) produce different results or when both tools fail to converge ($\sim 33\%$ of the BCG sample), we have assigned the morphological type (E/cD) relying on the visual inspection of the V-band images. The above procedure led us to classify most of the BCGs in our clusters (52 galaxies) as cDs (BCG_cD, hereafter). Table 1 reports the basic information about the BCGs in our sample, as well as some relevant properties of the host clusters.

In the clusters Abell 3395 and Abell 3556 the BCGs are quite off-centered with respect to the main concentration of galaxies, while the brightest objects belonging to such concentration (in both cases cD galaxies) turn out to be just slightly fainter than the corresponding BCGs. This motivated us to examine the very luminous galaxies in each cluster, searching for more non-BCG, cD candidates (nBCG_cD, hereafter). We found 14 additional cDs (including the two cDs previously mentioned in the central part of Abell 3395 and Abell 3556), all of them being just slightly fainter than the corresponding BCGs (see Table 2). Together with the 52 BCG_cDs in Table 1, these objects form a complete sample of 66 cD galaxies to be compared with the BCG_E sample and with the sample of normal Es extracted from the WINGS morphological catalogs (MORPHOT). We decided to include in the sample of Es just galaxies with absolute V magnitude $M_V < -19.5$ and cluster-centric distance less than $0.6R_{200}$ ¹. The first condition guarantees that the mor-

phological classification is robust enough, while the second condition is necessary to homogenize the photometric coverage of the clusters. Both conditions make the field contamination practically negligible. After having removed the BCG_Es and the cDs we are left with a final sample of 1024 Es.

In the framework of the WINGS survey, the surface photometry of several hundreds galaxies per clusters (those with projected area greater than ~ 22 arcsec² at the isophotal level corresponding to 2.5 times the r.m.s. of the background) has been obtained by using GASPHOT (Pignatelli et al. 2006; D’Onofrio et al. 2009). This purposely devised tool performs simultaneous best fitting of the major- and minor-axis growth light curves of galaxies with a 2D flattened Sersic-law, convolved with the appropriate (local) PSF. In the present paper we use for the shape analysis the axial ratios q_G of the Sersic model coming out from this best-fitting procedure. The reason for this choice is twofold: (i) since q_G is derived from a best-fitting procedure on the whole galaxy body, it is more stable than whatever isophotal axial ratio; (ii) since our result is at variance with RLP93 in that we find more flattened BCGs, and since q_G provides the lowest flattening among the various possible axial ratio estimates (as shown below; see Figure 1), our choice is a conservative one. Besides q_G , GASPHOT provides the axial ratio profiles of the galaxy isophotes. In Table 1 and 2 we report the isophotal axial ratios of the BCG and cD galaxies corresponding to the semi major-axes of 15, 30 and 60 kpc (q_{15} , q_{30} and q_{60}). It is worth noticing that q_G is not seeing-affected by definition, since it comes from the best fit of PSF-convolved Sersic models. Instead, this is not true for the isophotal axial ratios, at least in the innermost galaxy regions. However, we can assume the seeing influence to vanish for $D_m^{\text{isoph}}/\text{FWHM} > 3$, where D_m^{isoph} is the isophotal minor-axis. In the case of our (BCG_E+cD) sample, even in the worst seeing conditions (FWHM ~ 2 arcsecs; see Fasano et al. 2006) and for the most flattened objects ($b/a \sim 0.3$), the axial ratios of isophotes with semi-major axis > 10 arcsecs can be considered not seeing-affected. For most distant WINGS clusters ($z \sim 0.07$) this translates into ~ 13.5 kpc of isophotal semi-major axis. We conclude that all the isophotal axial ratios reported in Tables 1 and 2 are not seeing affected. We have also collected, for our (BCG_E+cD) sample, the axial ratios q_S from our photometric catalogs (Varela et al. 2009, SExtractor) and, if available, the axial ratios q_L from the LEDA Hypercat database (Paturel et al. 2003, see again Tables 1 and 2). The last ones are actually literature data statistically normalized to the isophote B_{25} , while the first ones are luminosity weighted axial ratios similar to those defined by RLP93, but referred to the whole galaxy body (the axial ratios from RLP93 are instead computed within ~ 13 kpc). All these additional estimates of q are useful to understand how the axial ratio definition could influence our results.

In Figure 1 the six different estimates of the axial ratios of our BCG_Es+cDs are compared among each another. The BCG_Es, BCG_cDs and nBCG_cDs are represented in the figure by white, black and grey (green in the electronic version) dots, respectively. For clarity, we will identify the panels with the numbers placed in bottom right. First of all, from plots 4, 5 and 9 it is clear that in our (BCG_E+cD) galaxy sample the flattening of the isophotes usually in-

¹ R_{200} is defined as the radius delimiting a sphere with interior mean density 200 times the critical density, approximately equal to the cluster virial radius. $0.6R_{200}$ roughly corresponds to R_{500} , whose interior mean density is 500 times the critical density. Only a few WINGS clusters have photometric coverage slightly smaller than $0.6R_{200}$ (Cava et al. 2009)

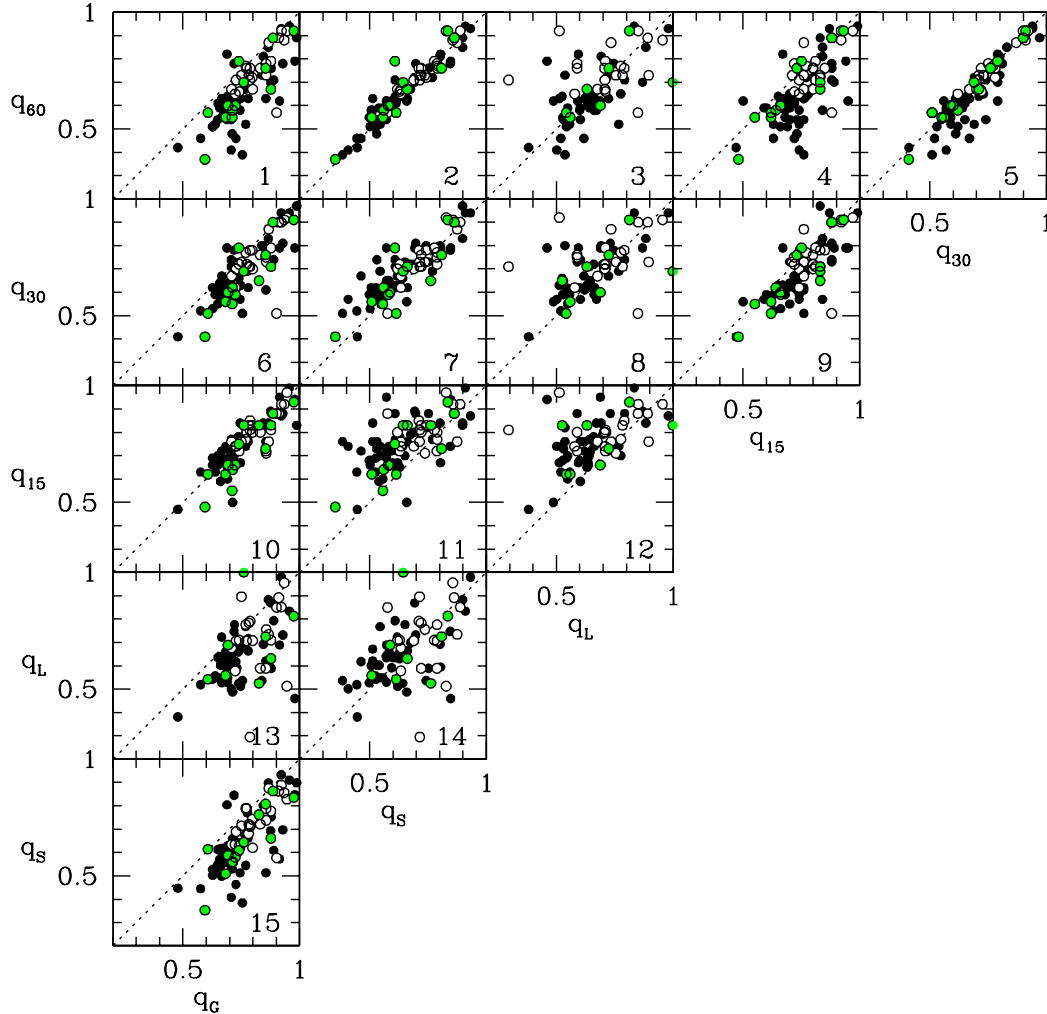


Figure 1. Comparison among different axial ratio measurements for the BCG_Es (white dots), BCG_cDs (black dots) and nBCG_cDs (grey dots; green in the electronic version) of the WINGS survey.

creases towards the outer galaxy regions. From plots 13 and 15 it is also evident that the axial ratios q_G are systematically larger than both q_S and q_L . From plots 2 and 10 the axial ratios q_S and q_G turn out to be consistent with q_{60} and q_{15} , respectively. Finally, the best consistency with q_L is found, although with a large scatter, in panel 8 with q_{30} .

3 THE AXIAL RATIO DISTRIBUTION OF BCG AND NORMAL ELLIPTICALS

In Figure 2 we compare the axial ratio distributions $\phi(q_G)$ of Es and BCGs (panel a), BCG_Es and cDs (panel b), BCG_Es and Es (panel c), nBCG_cDs and BCG_cDs (panel d). The full line (red in the electronic version of the paper) in the

top-leftmost panel of the figure, reports the axial ratio distribution of Es obtained by Fasano and Vio (1991), which turns out to be fairly in agreement with that of WINGS Es. The bottom panels show the corresponding cumulative distributions and report, in each case, the probability of the “null hypothesis” (i.e. that they are drawn from the same parent populations), according to the Kolmogorov-Smirnov (KS) statistics. Figure 2 (panel a) shows that the distribution $\phi(q_G)$ of BCGs looks strongly different from that of normal ellipticals, the BCGs being systematically flatter than Es.²

² Note that our sample of Es includes galaxies with absolute V magnitude brighter than -19.5 : a rather faint cutoff, indeed. Since luminous Es ($M_B < -20$, i.e. roughly $M_V < -21$) are found to be

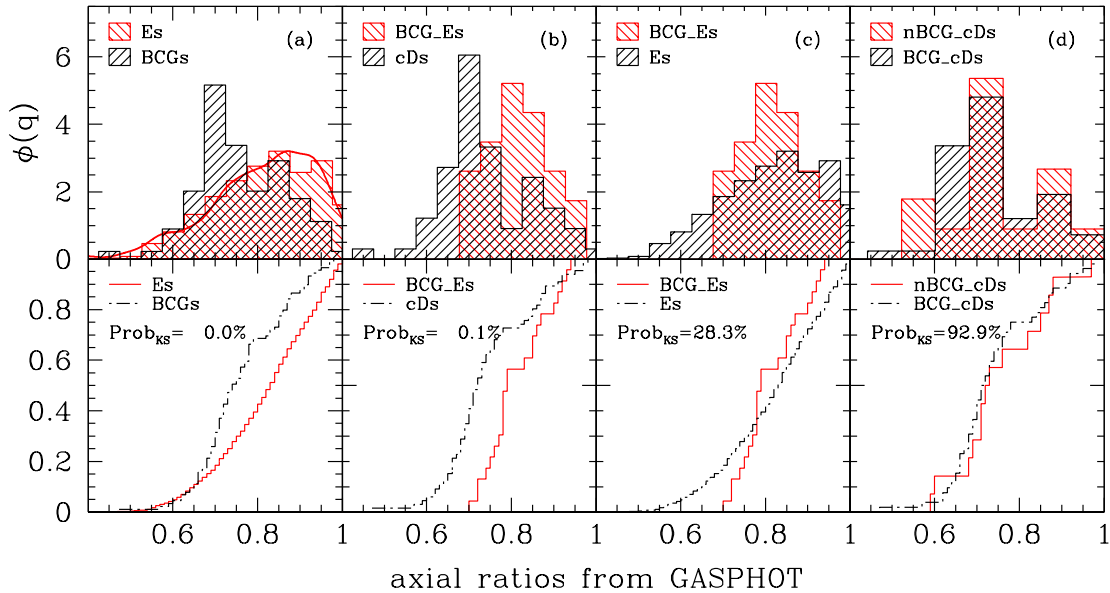


Figure 2. Differential (top panels) and cumulative (bottom panels) axial ratio distributions in the WINGS survey: comparisons between Es and BCGs (leftmost panels; red and black, respectively), BCG_Es and cD galaxies (panel b), BCG_Es and Es (panel c), nBCG_cDs and BCG_cDs (rightmost panels). The bottom panels also report the probability that they are drawn from the same parent populations, according to the KS statistics.

This result is strongly at variance with that obtained by RLP93, who conclude that BCGs and Es share the same axial ratio distribution. Trying to interpret this quite evident discrepancy, we could invoke the different procedures adopted to measure the axial ratios. However, we should note that, among the six different values of q we have collected for our BCGs sample, the one we use to get our distributions (q_G) is by far the one producing the least flattened galaxies (see Figure 1), being also quite consistent with q_{15} (the same outermost isophote used by RLP93). One could object that, with respect to our method, the one used by RLP93 to measure q tends to overweight the inner galaxy regions, which for the BCGs are well known to be rounder than the outer ones (see again Figure 1). However, we should also note that our SExtractor estimates, even if computed in a fashion similar to RLP93, are actually in fair agreement with the isophotal axial ratios at 60 kpc (q_{60} ; see plot 2 in Figure 1), which give the flattest distribution. Again, one should object that our SExtractor estimates are computed on the whole galaxy body, while the RLP93 ones refer to the region inside the 15 kpc. In any case, it is worth stressing that, using the same axial ratio definition (q_G), we get very different q distributions for BCGs and normal Es. At this point, the discrepancy between our result and that obtained by RLP93 remains rather puzzling. In Section 5 we will present a strong guess about the origin of such discrepancy. For now we just note that, besides the result concerning the shape difference between BCGs and Es, the Figure 2 is telling us something else: (i) cD galaxies are significantly

rounder (Tremblay and Merritt 1996), had we adopted a brighter cutoff, the difference between the axial ratio distributions of Es and BCGs would have been even larger.

flatter than BCG_Es (panel b), thus implying that the BCGs do not constitute an homogeneous class of objects; (ii) the distribution of BCG_Es does not significantly differ from that of normal Es (panel c); (iii) the cD galaxies have a unique, characteristic shape distribution, regardless of the luminosity ranking in the cluster (panel d). Note that this result basically justifies why in panel b BCG_Es are compared with the whole sample of cDs rather than just with BCG_cDs.

4 INTRINSIC SHAPES OF BCG AND NORMAL ELLIPTICALS

4.1 Technicalities

Following RLP93, hereafter we assume that the intrinsic isoluminosity surfaces of a galaxy are similar coaxial ellipsoids with axis lengths in the ratio $1:\beta:\gamma$, with $1 \geq \beta \geq \gamma$, β and γ being the intrinsic axial ratios of the galaxy. Moreover, following Franx et al. (1991), we quantify the triaxiality of galaxies through the parameter $T = (1 - \beta^2)/(1 - \gamma^2)$ (which becomes 0/1 for perfectly oblate/prolate bodies) and illustrate the results in the (β, γ) plane (see also Figure 1 in Kimm and Yi 2007).

To explore the probability density function $\psi(\beta, \gamma)$ of the intrinsic axial ratios for a given sample of galaxies (hopefully of the same morphological family), we deproject the distribution of their observed axial ratios $\phi(q_G)$ using the iterative *rectification* algorithm devised by Lucy (1974), in particular its equations (13), (14) and (17). In our case the equation (17) in Lucy (1974) becomes:

$$\psi^{r+1}(\beta, \gamma) = \frac{1}{N} \sum_{n=1}^N \frac{\psi^r(\beta, \gamma)}{\phi^r(q_n)} P[q_n | \beta, \gamma, \epsilon(q_n)], \quad (1)$$

where N is the size of the galaxy sample and r is the iteration number. In this equation the r -th estimation of $\phi(q)$ is obtained through the equation:

$$\phi^r(q_n) = \int \int \psi^r(\beta, \gamma) P[q_n | \beta, \gamma, \epsilon(q_n)] d\beta d\gamma, \quad (2)$$

where $P[q | \beta, \gamma, \epsilon(q)]$ is the probability that an ellipsoid with intrinsic axial ratios β and γ is observed with apparent axial ratio q , assuming a random space orientation and the *r.m.s.* of the errors (ϵ) in the q measurements to be a function of q itself.

The iterative machine requires a first guess $\psi^0(\beta, \gamma)$ of the probability density function we are exploring and a choice of the error function $\epsilon(q)$. According to Fasano et al. (1993, see Figure 1 and equation 1 therein), we assume the last one to be a linear function of q . In particular, after some statistical comparison among literature data, we decided to use the equation: $\epsilon(q) = 0.05(1+q)$. Concerning the choice of $\psi^0(\beta, \gamma)$, we tried different analytical functions, concluding the most flexible and robust guess to be a confined normal function, bi-variate in the two quantities γ and T (triaxiality). In this way, the first guess of ψ requires eight parameters (upper and lower limits, central value and σ of the normal function, for both T and γ). In general, the lower limits of β and γ could be assumed to be 0.3 (strongly elongated, prolate galaxies) and 0.05 (very thin disk galaxies), respectively. Actually, since we are dealing with Es and cDs galaxies, we are allowed to explore ψ down to $\gamma \sim 0.3$.

The left and right panels of Figure 3 illustrate, on the plane (β, γ) , the result of the previously outlined bi-variate Lucy's rectification procedure for the WINGS samples of Es (top panels) and BCG galaxies (bottom panels). For each galaxy sample, we first tried to perform the rectification without any assumption about the initial guess ($\psi^0 \equiv \text{const.}$). The distributions obtained in this way for the two galaxy samples are shown in the left panels of the figure. Then, we use such *blind* runs to refine the results by providing more realistic initial guesses ψ^0 , expressed as confined, bi-variate normal functions of γ and T . The results of this refined de-projection procedure are illustrated in the right panels of Figure 3. For each sample, the ideal number of algorithm iterations has been chosen relying upon numerical simulations recording the cycle number for which the provisional and the input ψ distributions display the best mutual agreement. Such ideal number turns out to depend on the sample size, being also usually greater than the corresponding values found for the one dimensional application of the Lucy algorithm (see Noerdlinger 1979 for perfectly oblate and prolate cases).

We are obviously aware that, since $\phi(q)$ is a function of one variable, it cannot uniquely determine the function $\psi(\beta, \gamma)$. This means that the previously devised Lucy algorithm can, in principle, produce totally wrong ψ distributions which perfectly reproduce the observed distributions of $\phi(q)$. This actually happens for certain ψ distributions (i.e. disk galaxies) when the first guess ψ^0 is lacking or far from the true ψ . In our case, extensive numerical simulations have shown that, even in default of the first guess ($\psi^0 \equiv \text{const.}$), the iterative Lucy machine is able to recover reasonably well

the parent ψ distribution. However, in order to obtain an objective, independent check of this conclusion, we have used a procedure similar to that adopted by RLP93. In practice, assuming a gaussian (bi-variate) functional form of $\psi(\beta, \gamma)$, we have scanned the (β, γ) space with the gaussian peak, choosing in each point the values of the two standard deviations which, according to the KS statistic, produces the best agreement with the observed axial ratio distribution. In this way, we have produced a grid of KS probabilities that the $\phi(q)$ resulting from the random projection of the local gaussian ψ is drawn from the same parent population of the observed axis ratio distribution. The middle panels of Figure 3 illustrate the results of such procedure for both Es (top panel) and BCG galaxies (bottom panel). The impressive overlap between the regions where the distributions $\psi(\beta, \gamma)$ peak according to the Lucy's algorithm (left and right panels) and the regions where is highest the probability from KS statistics (middle panels), clearly indicates that, in our specific case, the bi-variate version of the Lucy's algorithm works fairly well, even when it is run in blind mode ($\psi^0 \equiv \text{const.}$). We also note that the distribution of KS probabilities for the normal ellipticals in our sample (mid-top panel in Figure 3) is quite similar to the corresponding distribution obtained by RLP93 (see Figure 5 therein).

4.2 Results

Figure 3 provides us with a robust indication about the intrinsic shapes distributions of both Es and BCGs. Just as expected from the observed axial ratio distributions in Figure 2, they turn out to be quite apart from each other. In particular, there is a clear tendency of the BCGs towards strong prolate configurations peaked at $\beta \sim \gamma \sim 0.67$, while the Es tend to share almost uniformly the whole range of triaxiality, with a slight tendency toward prolateness.

Figure 4 is similar to the previous one, but it refers to the comparison between cD and BCG_E galaxies in our sample. This figure shows that the strongly prolate shape we found for the whole population of BCGs (see lower panels of Figure 3) is entirely due to the sub-sample of cD galaxies. Moreover, in spite of the paucity of the BCG_E sample (responsible for the wide distribution of the KS probabilities in the mid-bottom panel of Figure 4), we note the similarity between the ψ distributions obtained for Es and BCG_Es in the top-right and bottom-right panels of Figures 3 and 4, respectively.

The results illustrated in Figures 3 and 4 suggest that cD galaxies actually constitute a foreign body inside the global population of cluster early-type galaxies, at least as far as the axial ratio distribution is concerned. To give more robust statistical support to this suggestion, we have obtained the axial ratio distributions of the second- and third-luminosity-ranked galaxies in our cluster sample and we have compared them with the corresponding distributions of Es, BCGs and cDs. The black dots in Figure 5 report, for the cD galaxies and for the first three ranked ellipticals in the WINGS clusters, the KS probabilities that the observed $\phi(q)$ of each galaxy sample and that of the normal Es are drawn from the same parent population.

From this figure it is evident that the $\phi(q)$ distributions of the 2nd- and 3th-ranked galaxy samples (of which cDs just represent a very small fraction) are undistinguishable from

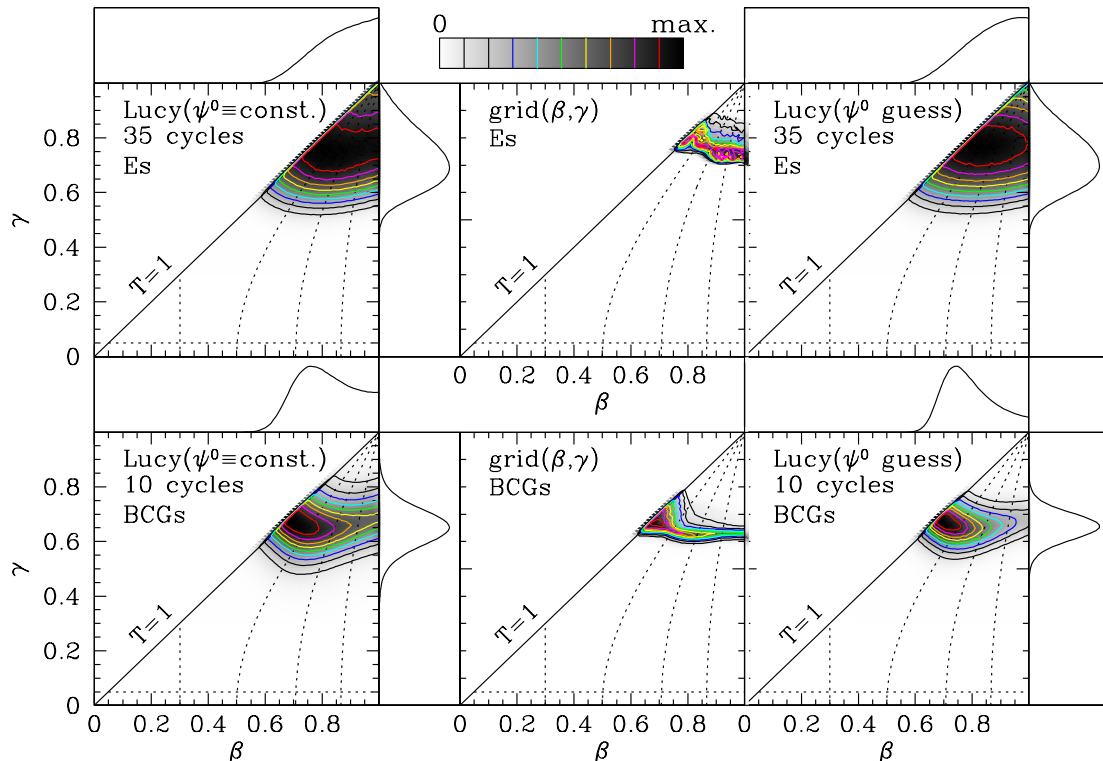


Figure 3. *left and right panels:* comparison between the probability distributions $\psi(\beta, \gamma)$ obtained with the Lucy algorithm for the sample of normal ellipticals (top panels) and BCG galaxies (bottom panels) in the WINGS survey. The left panels in the figure are obtained in blind mode (initial guess $\psi^0 \equiv \text{const.}$), while in the right panels we let ourselves be guided by the results of the blind tests to guess ψ . *middle panels:* distributions of the KS probabilities obtained, for normal ellipticals (top panel) and BCG galaxies (bottom panel), scanning the (β, γ) space with a bivariate, gaussian ψ and comparing in each point the expected $\phi(q)$ with the observed axis ratio distribution (see text). The grey tones and the isophotes in each panel illustrate the density levels (see the uppermost grey-tone scale). For the left and right panels the marginal distributions of ψ onto the β and γ axes are shown in the upper and right part of each panel, respectively. Finally, in each panel the loci of $T=0.25, 0.5, 0.75$ are reported with short-dashed lines.

that of Es, while for the whole sample of BCGs one can exclude the hypothesis of common parent population between these samples and the global elliptical sample. Nevertheless, in analogy with the ψ distributions (see Figures 3 and 4), if we consider just the BCG_E sample (red, empty dot in the figure), again its $\phi(q)$ distribution turns out to be undistinguishable from that of normal ellipticals. This confirms our previous claim about the peculiar intrinsic shape of cDs inside the family of early-type cluster galaxies.

5 DISCUSSION

5.1 Cluster X-ray luminosity and BCGs shapes

The last mentioned result could also be enough to explain the discrepancy between our finding and the result from RLP93. In fact, the fraction of clusters containing at least one cD galaxy in our sample is $\sim 75\%$ (56 clusters). Instead, using the morphological information provided by the *Nasa Extragalactic Database* (NED), we were able to associate cD types to just $\sim 26\%$ of the BCGs in the RLP93 sample. Even though most of the BCGs in the RLP93 sample are actually lacking NED morphological information, there is an indication that the BCG_Es (less flattened) dominate the RLP93 sample, while the cDs (more flattened) dominate our sam-

ple of BCGs. This circumstance can easily justify the above discrepancy.

Trying to explain the remarkable difference in the cD frequency between the two cluster samples, we suggest it could be due to the different cluster selection criteria. In fact, WINGS clusters have been selected, in the redshift range 0.04–0.07, to be powerful X-ray emitters ($\text{Log}L_X > 43.3 \text{ erg s}^{-1}$). Conversely, the RLP93 sample, even spanning a similar range of redshift, does not obey this criterion. Therefore, the different percentages of cDs could be easily explained if cD galaxies preferentially resided in X-ray powerful clusters. Since we were not able to find in the literature any clear indication about such a possibility, we tested it in our cluster sample. From Figure 6 the tendency of cDs to preferably reside in X-ray powerful clusters is confirmed with high significance ($>99\%$) if just BCG_cDs are considered (right panel), while the significance is slightly lower if we also consider nBCG_cDs (left panel). Such small difference of significance might suggest that the above tendency is stronger for BCG_cDs than for nBCG_cDs. However, the KS test applied to the X-ray luminosity distributions of clusters hosting BCG_cDs and nBCG_cDs turns out to be inconclusive ($\text{Prob}_{KS} \sim 50\%$).

Since cDs are known to be specially luminous and sizeable even among the BCGs, the previous result about their

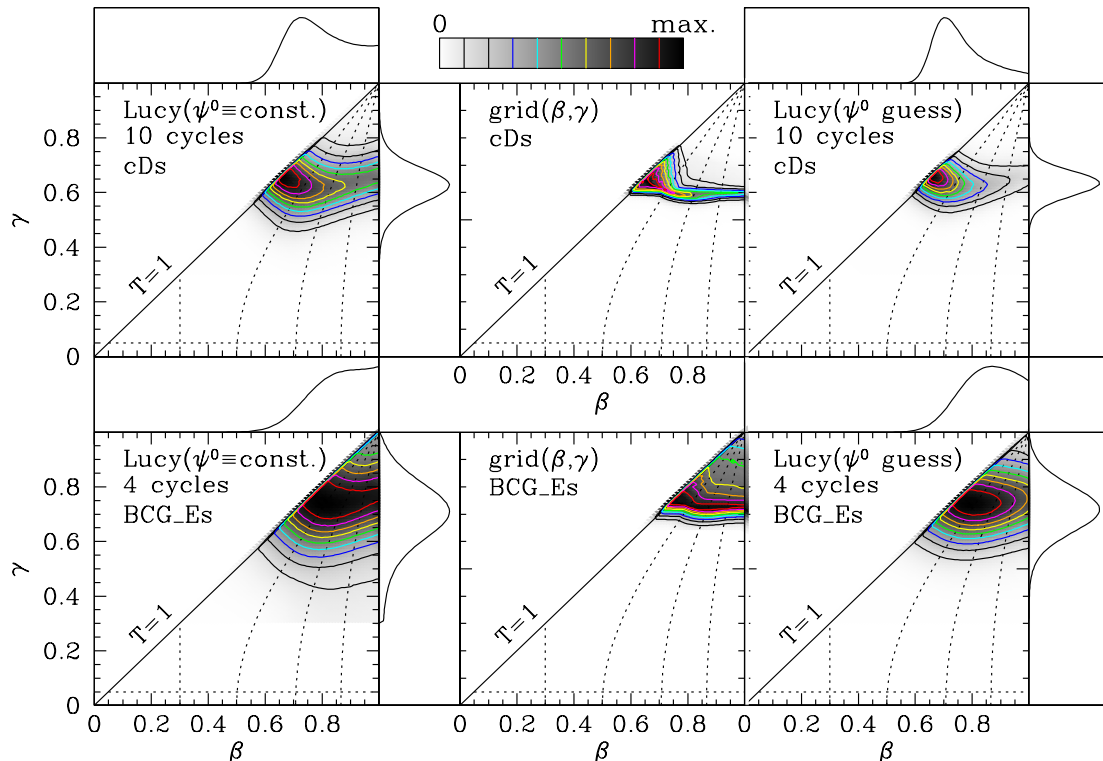


Figure 4. Comparison between the probability distributions $\psi(\beta, \gamma)$ for the sample of BCGs (bottom panels) and cD galaxies (top panels) in the WINGS survey. See the caption of the previous figure for details.

preference to reside in X-ray powerful clusters suggests that a correlation should exist between the BCGs absolute magnitude (or size) and the cluster X-ray luminosity (or mass). Actually, similar correlations have been already reported in the literature (Burke et al. 2000; Brough et al. 2002; Katayama et al. 2003; Lin and Mohr 2004; Brough et al. 2005; Whiley et al. 2008). Figure 7 show the above correlations for the WINGS cluster sample. In this figure the BCGs luminosities are expressed in K-band absolute magnitudes from 2MASS (see Table 1) and the virial masses of the clusters are computed from the velocity dispersion of galaxies inside them (both these quantities are reported in Table 1). The radii of the BCGs in the right panel of the figure are equivalent radii ($\sqrt{a \times b}$) computed from the threshold area reported in the photometric WINGS catalogs (Varela et al. 2009). Even if not fully homogeneous in the surface brightness level, this kind of size measurement turns out to be useful to sample the outer shapes of the BCGs. In Section 5.2 these shapes will be compared with those of dark-matter halos from Λ CDM N -body simulations, which are hardly recoverable in their inner part, due to the insufficient resolution. Besides the Pearson correlation coefficients, Figure 7 reports the probabilities of the null hypothesis (no correlation). Moreover, the right panel of the figure also report the linear fit (r.m.s. ~ 0.13):

$$\text{Log}(R_{BCG}^{kpc}) = 0.37(\pm 0.056) \times \text{Log}(\text{Mass}_{Clus.}) - 3.67(\pm 0.81) \quad (3)$$

which we use in the analysis of the Λ CDM N -body simulations (see next section).

5.2 Dark-matter halos N -body simulations

It is interesting to compare the distribution of BCG axial ratios in the WINGS survey with that of the central part (at BCGs scale) of cluster-sized dark-matter halos obtained with Λ CDM N -body simulations. In the Λ CDM scenario, small dark matter haloes form first and grow subsequently to larger structures via accretion and merging processes. Such processes are generally anisotropic, so that dark matter halos are expected to be non-spherical. A number of papers have been devoted to the shape analysis of dark-matter halos (see references in Section 1). Recently some studies, with both simulations and comparison with observations, have shown the importance of the total mass in determining the final halo shape. Indeed, it has been noted that the flattening increases with halo mass, becoming more pronounced at $M_{vir} > 10^{14} M_{\odot}$ (see, among others, Wang et al. 2008; Macciò et al. 2008; Flores et al. 2007). Moreover, by using a set of hydrodynamical simulations on the cluster mass scale, Kazantzidis et al. (2004) and Gottlöber and Yepes (2007) find that gas cooling makes the central parts of the halos more round. Thus, one should expect that dark matter halos of galaxy clusters are even more elongated than the embedded central BCGs. Finally, both dynamical models (West 1994) and N -body simulations (Dubinski 1998) suggest that halos are preferentially aligned with primordial filaments, as well as with the elongation of the host galaxy cluster.

A truly realistic comparison between our observations and numerical simulations would require an accurate modelling of hydrodynamics, radiative cooling, star formation and energy feedback from SNe and AGNs, high enough mass

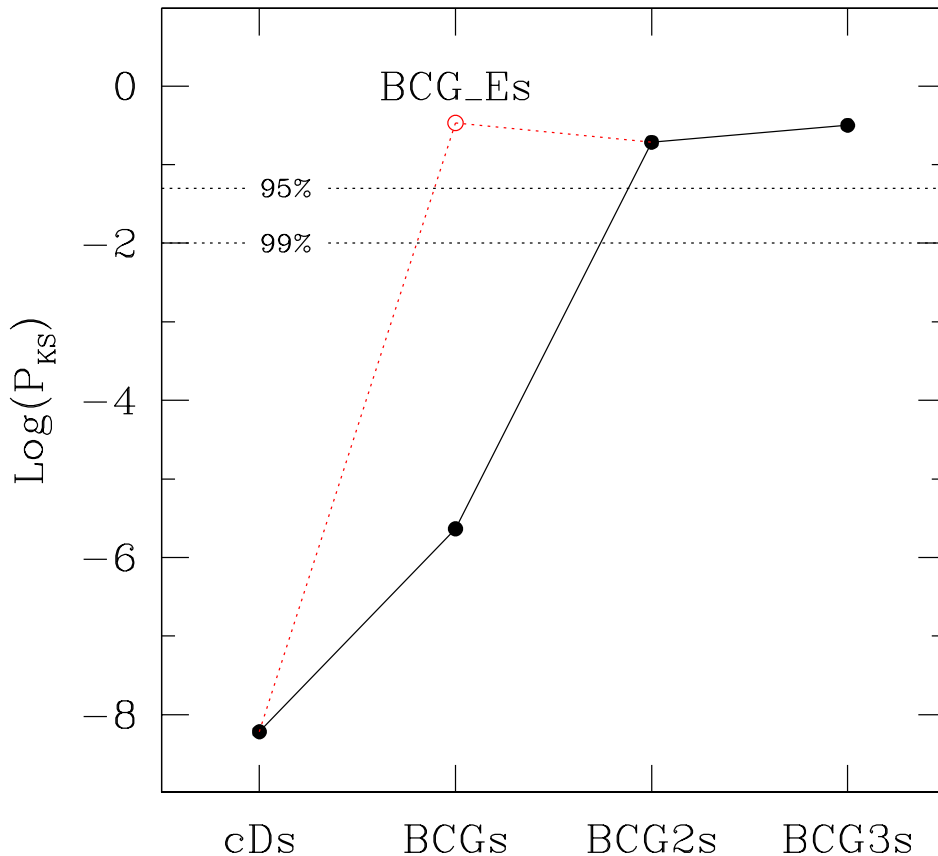


Figure 5. KS probabilities relative to the comparisons of the axial ratio distribution of Es with those of cD galaxies and of the first three luminosity ranked ellipticals in the WINGS cluster. The red dot refer to the BCG_E sample (non cDs).

and force resolution, and full control over the numerical effects. Unfortunately, our incomplete knowledge of the details of galaxy formation, and the insufficient computational capabilities, make this impossible as of today. We must thus rely on the more robust - although simpler - modelling of the dark-matter distribution. In order to make such a comparison still meaningful, we chose to compare the intrinsic shape of BCGs with that of the innermost region of cluster-sized dark matter halos extracted from a cosmological simulation.

We compare the intrinsic shape of our BCGs with that of the innermost region of cluster-sized dark matter haloes extracted from GIF2 simulation (see Gao et al. 2004, hereafter GIF2)³, a cosmological N -body simulation of the concordance Λ CDM model, performed with 400^3 dark-matter particles in a box of 110 Mpc/h on a side. Halos were identified at redshift $z = 0$ using a spherical overdensity criterion, cut at the Λ CDM virial overdensity: $\Delta_{vir} = 324$ (Eke et al. 1996). Among these we selected 3510 halos with

virial mass above $10^{14} M_{\odot}$, appropriate to compare to the WINGS galaxy clusters (see lower mass limit in right panel of Figure 7).

Given the discrete structure (particles) of the matter distribution in the N -body simulations, we have used an iterative procedure to obtain the shapes of the halo isodensity shells. As a first guess, we calculated the main axes of the dark-matter particle distribution inside a sphere of radius R_{BCG} , where R_{BCG} is randomly assigned from equation (3), assuming a gaussian scatter (see also right panel of Figure 7). Then, keeping the volume of the region fixed, we define a new ellipsoidal region using these axes and obtain new values for the main axes. We iterate this procedure until the main axes converge to a stable value, which we assigned to the dark matter halo as representative of its “simulated” BCG. The typical dark matter overdensity at the radii considered in this procedure is of order 10^5 times the background density. In the upper-left panel of Figure 8 we plot the distribution of the intrinsic axial ratios for the dark matter halo regions thus identified.

³ data publicly available at http://www.mpa-garching.mpg.de/Virgo/data_downloads/. The comparison of this plot with Figures 3 and 4, led

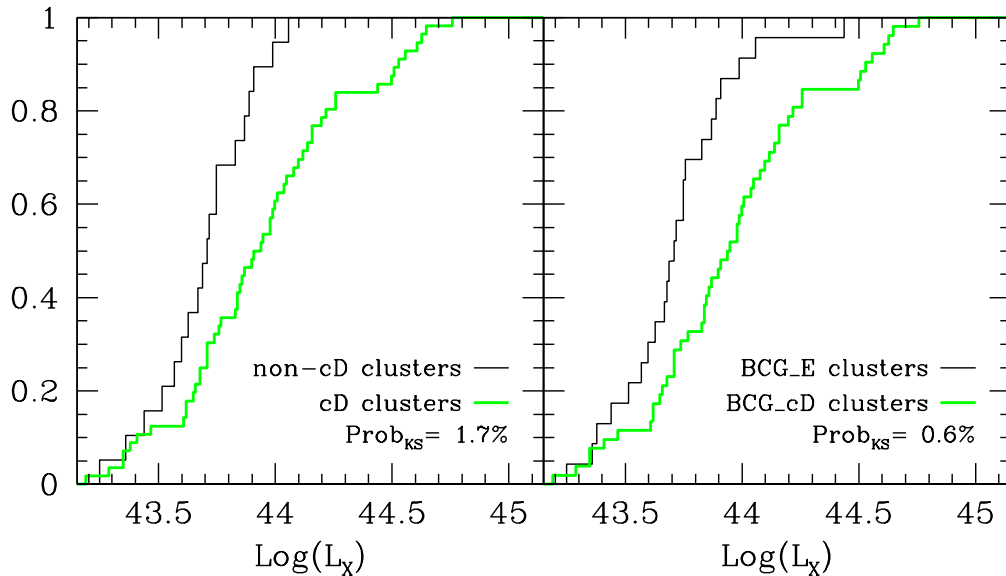


Figure 6. *Left panel:* comparison between the X-ray luminosity distributions of WINGS clusters hosting (thick grey line; green in the electronic version) and not-hosting (thin black line) at least one cD galaxy (even if not BGC). *Right panel:* comparison between the X-ray luminosity distributions of WINGS clusters with (thick grey line; green in the electronic version) or without (thin black line) BCG_cDs (even if not BGC). In each panel the probability that the distributions under analysis are drawn from the same parent population according to the KS statistics is reported.

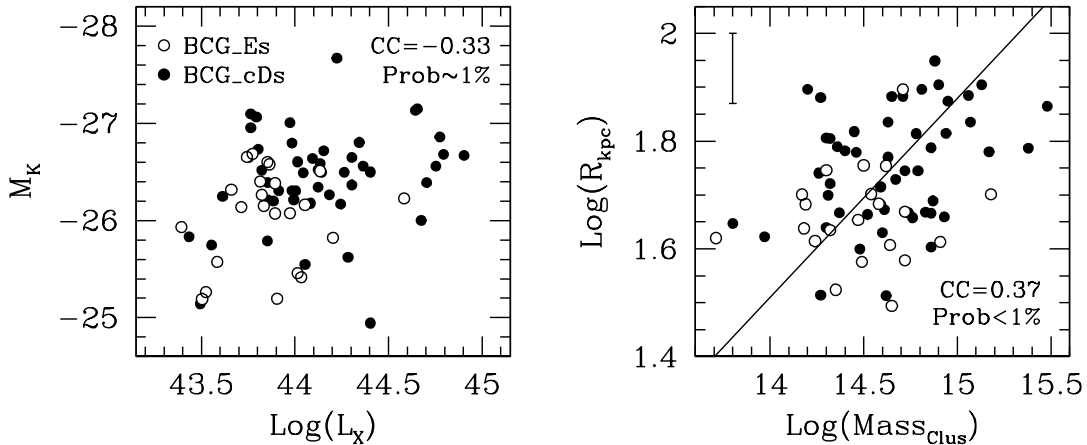


Figure 7. *Left panel:* correlation between absolute K-band magnitude (from 2MASS) of the BCGs in the WINGS survey and the cluster X-ray luminosity. *Right panel:* correlation between the virial cluster mass and the equivalent radius (in kpc) of the BCG, derived from the threshold area. The error bar in the left-upper part of the plot shows the *r.m.s.* of the correlation (see eq. 3 and text for details)

us to the conclusion that dark matter halos are even more elongated and strongly prolate than our BCGs/cDs galaxies. However, it is worth recalling that the axial ratios in Figures 3 and 4 refer to the effective isophotes, while the size distribution we use to extract the intrinsic shapes of dark-matter halos in the GIF2 simulation has been calibrated (right panel of Figure 7 and eq. 3) on the threshold isophotes of the BCG sample, which, as seen in panel 15 of Figure 1, tend to be flatter than the effective isophotes. To obtain

a more consistent comparison, in the remaining panels of Figure 8 we illustrate the results of the previously outlined rectification procedure (with initial guess $\psi^0 \equiv \text{const.}$) on our samples of BCGs (upper-right), BCG_Es (bottom-left) and cDs (bottom-right), when the axial ratios of the threshold isophotes (q_S) are used instead of the effective axial ratios (q_G). Even if in this case the BCGs tend to be more elongated than in the case of the effective isophote, still they turn out to be rounder when compared to the dark matter halos, giv-

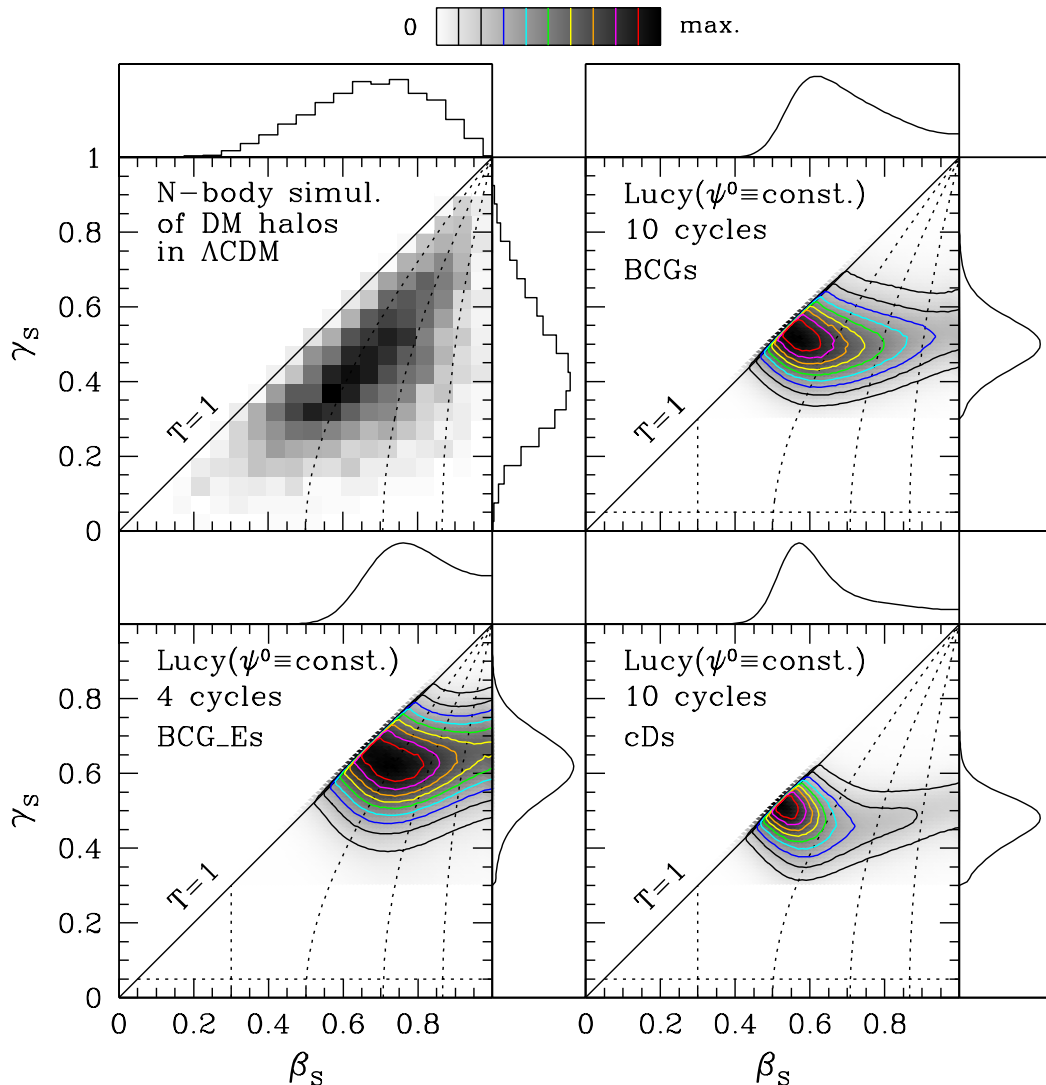


Figure 8. Distribution of the intrinsic axial ratios for the sample of dark-matter halos extracted from the GIF2 N -body simulation (upper-left panel), compared with the corresponding distributions (β_s, γ_s) obtained deprojecting the distributions of the threshold isophotes q_s for our samples of BCGs (upper-right), BCG_Es (bottom-left) and cDs (bottom-right).

ing support to the results of Kazantzidis et al. (2004) and Gottlöber and Yepes (2007) about gas cooling effects on the central parts of simulated galaxy clusters.

5.3 The shapes of BCGs and their evolution

In our sample of BCGs, the distributions of many quantities indicate that BCG_cDs are systematically different from BCG_Es (stronger flattening, higher mass and larger size, preference to reside in massive and X-ray powerful clusters; see Figures 2, 6 and 7). However, the only statistically robust differences concern the shapes ($P_{KS} < 0.001$) and the X-ray luminosity of the host clusters ($P_{KS} < 0.01$).

The tendency of cDs to reside in more X-ray power-

ful clusters and their strong prolateness when compared to BCG_Es, together with the (even more) elongated and prolate shapes of the inner parts of cluster-sized, simulated dark matter halos (see Figure 8), could give interesting hints for understanding the formation histories of both the BCGs and the host clusters themselves.

A detailed discussion about what the above mentioned results, together with those emerging from recent dynamical and stellar population studies of BCGs, imply about their formation and evolution, is beyond the scope of this paper. We actually plan going deeper into this topic in a forthcoming paper, using the whole information on BCGs from the WINGS database. We just provide here a few specula-

tions, also based on the results of some recent analyses in the literature.

Stott et al. (2008), Whiley et al. (2008) and Collins et al. (2009) have demonstrated that the stellar population in BCGs has been mostly in place (90% of the total mass) since $z \sim 2$ and that, contrary to the predictions of cosmological simulations and hierarchical-based galaxy formation models (Bower et al. 2006; De Lucia and Blaizot 2007), the BCGs are almost fully assembled a few billion years after the Big Bang. On the other hand, converging indications exist that the most luminous (and massive) BCGs may often display signatures of most recent star formation (blue-cores), likely related to the presence in the host clusters of cooling flows and X-ray luminosity excess with respect to the average $L_X - T_X$ relation (Bildfell et al. 2008; Loubser et al. 2009). The most luminous BCGs are also claimed by Bildfell et al. (2008) to be closer to the peaks of the cluster X-ray emission with respect to the less luminous BCGs. Finally, Coziol et al. (2009) show that most BCGs are not at rest in the potential well of their clusters, suggesting a merging-group scenario, where BCGs formed first in smaller subsystems and clusters formed more recently from the mergers of many such groups. They also claim that the relative peculiar velocity inside the cluster (i.e. the difference between specific and average velocity, normalized to the velocity dispersion) is lower for BCG_cDs than for BCG_Es.

All these claims, together with the findings reported in the present paper and the fact that the BCG_cDs are (on average) more luminous and massive than the BCG_Es, point toward a scenario in which BCG_cDs and BCG_Es have experienced quite different formation and evolution processes, although both have been assembled very early (old stellar populations). In particular, the BCG_cDs could have been formed close to the centers of quite sizeable and prolate (Gottlöber and Yepes 2007) dark-matter halos, dominant with respect to the surrounding ones and progenitors of the most massive, present day halos (small displacement of the BCGs from the cluster centers and small relative peculiar velocity). In this context, considerable and prolonged accretion of material through cooling flows (enhanced X-ray emission) and/or dry minor mergers (Bernardi 2009), associated with modest star formation (blue-cores), could have been at work from preferential directions (the streaming filaments), thus producing a puffing up process along them, leading to the formation of extended and elongated halos (cD morphology). On the other side, the BCG_Es could have formed inside group-sized halos, not much larger than the surrounding ones. Later on, according to the scenario proposed by Coziol et al. (2009), the galaxy groups originating the BCG_Es could have merged with many other groups, to form cluster-sized systems. In this context, one should expect the BCGs to show very low or absent star formation, to have larger displacement from the cluster centers and larger relative peculiar velocities compared to the BCG_cDs. Moreover, in this case the host clusters are expected to show less frequently cooling flows and to be less powerful X-ray emitters.

6 SUMMARY

In this paper we have analysed the apparent axial ratio distributions of the BCGs and of the normal ellipticals in our sample of 75 galaxy clusters from the WINGS survey. Most BCGs in our clusters (52) have been classified as cD galaxies. The cD sample has been completed by 14 additional cDs (non-BCGs) we found in our clusters. We have deprojected the apparent axial ratios distributions of BCGs, cDs and normal ellipticals using a bi-variate version of the rectification Lucy's algorithm. Since in our case the bi-variate distribution of the intrinsic axial ratios cannot be uniquely determined by the univariate distribution of the apparent axial ratios, we have used an independent Monte-Carlo technique to support the results of the Lucy's algorithm. Finally, we have used the GIF2 Λ CDM N -body simulations of cluster-sized, dark-matter halos, to compare the intrinsic shapes of the inner part (BCG-sized) of halos with those of the observed BCGs.

The main conclusions are the following:

- The *normal* Es have triaxial shape, the triaxiality parameter sharing almost evenly the (β, γ) space (with a slight preference for prolateness) and the γ parameter peaking around 0.7. In this case, our result is fairly in agreement with that provided by RLP93;
- the normal BCGs (non-cDs) and the second and third luminosity ranked Es in the clusters do not differ from the global population of Es as far as the distribution of the intrinsic shapes is concerned;
- the cDs have triaxial shape too. However, in this case the tendency towards prolateness is very strong and the preferred values of β and γ are significantly lower (~ 0.6) than the peak values found for Es;
- since more than 2/3 of the BCGs in our sample are cD galaxies, the results of the shape analysis for our global sample of BCGs are similar to those obtained for cDs (prolateness, significant difference from the Es);
- this result turns out to be strongly at variance with the conclusions given by RLP93, who found that BCGs and Es have similar apparent and intrinsic axial ratio distributions. This discrepancy is hardly attributable just to systematic differences in the axial ratios measurements;
- since we find that, among BCGs, cDs are quite flatter than non-cDs, and since the WINGS clusters have been selected to be X-ray powerful, while the RLP93 clusters haven't, we suggest the above discrepancy to be caused by a preference of cDs to reside in X-ray emitting clusters. Actually, this hypothesis turns out to be supported by the comparison between the X-ray luminosity distributions of the cD and non-cD clusters in our sample;
- the prolateness of the BCGs (in particular of the cDs) could reflect the shape of the associated dark-matter halos, according to the GIF2 N -body data.

ACKNOWLEDGMENTS

The simulations in this paper were carried out by the Virgo Supercomputing Consortium using computers based at Computing Centre of the Max-Planck Society in Garching and at insitute for Computational Cosmology. The data are publicly available at www.mpa-garching.mpg.de/NumCos.

We thank Paola Mazzei and Marisa Girardi for useful discussions. We are also grateful to the anonymous referee, whose comments allowed us to improve the paper.

REFERENCES

- Allgood, B., Flores, R. A., Primack, J. R., Kravtsov, A. V., Wechsler, R. H., Faltenbacher, A., & Bullock, J. S. 2006, *MNRAS*, 367, 1781
- Bailin, J., & Steinmetz, M. 2005, *ApJ*, 627, 647
- Bak, J., & Statler, T. S. 2000, *AJ*, 120, 110
- Beers, T. C., & Geller, M. J. 1983, *ApJ*, 274, 491
- Bernardi M., Hyde J. B., Sheth R. K., Miller C. J., & Nichol R. C. 2007, *AJ*, 133, 1741
- Bernardi M. 2009, *MNRAS*, 395, 1491
- Bertin, E., & Arnouts, S. 1996, *A&A*, 117, 393
- Bett, P., Eke, V., Frenk, C. S., Jenkins, A., Helly, J., & Navarro, J. 2007, *MNRAS*, 376, 215
- Bildfell, C., Hoekstra, H., Babul, A., & Mahdavi, A. 2008, *MNRAS*, 389, 1637
- Bower, R. G., Benson, A. J., Malbon, R., Helly, J. C., Frenk, C. S., Baugh, C. M., Cole, S., & Lacey, C. G. 2006, *MNRAS*, 370, 645
- Brough, S., Collins, C. A., Burke, D. J., Mann, R. G., & Lynam, P. D. 2002, *MNRAS*, 329, L53
- Brough, S., Collins, C. A., Burke, D. J., Lynam, P. D., & Mann, R. G. 2005, *MNRAS*, 364, 1354
- Burke, D. J., Collins, C. A., & Mann, R. G. 2000, *ApJLett.*, 532, 105
- Carter, D. & Metcalfe, N. 1980, *MNRAS*, 191, 325
- Cava, A., et al. 2009, *A&A*, 495, 707
- Cava, A., et al. 2010, in preparation
- Cole, S., & Lacey, C. 1996, *MNRAS*, 281, 716
- Collins, C. A., et al. 2009, *nature*, 458, 603
- Conselice, C. J., 2003, *ApJS*, 147, 1
- Coziol, R., Andernach, H., Caretta, C. A., Alamo-Martinez, K. A., & Tago, E. 2009, *AJ*, 137, 4795
- De Lucia G., & Blaizot J. 2007, *MNRAS*, 375, 2
- Desroches, L. B., Quataert, E. Ma, C. P., & West, A. A. 2007, *MNRAS*, 377, 402
- D'Onofrio, M., et al. 2009, in preparation
- Dubinski, J. 1998, *ApJ*, 502, 141
- Ebeling, H., Voges, W., Bohringer, H., Edge, A. C., Huchra, J. P., & Briel, U. G. 1996, *MNRAS*, 281, 799
- Ebeling, H., Edge, A. C., Bohringer, H., Allen, S. W., Crawford, C. S., Fabian, A. C., Voges, W., & Huchra, J. P. 1998, *MNRAS*, 301, 881
- Ebeling, H., Edge, A. C., Allen, S. W., Crawford, C. S., Fabian, A. C., & Huchra, J. P. 2000, *MNRAS*, 318, 333
- Edge, A. C., & Stewart, G. C. 1991, *MNRAS*, 252, 428
- Eke, V. R., Cole, S., Frenk, C. S., & Navarro, J. F. 1996, *MNRAS*, 282, 263
- Fabian, A. C. 1994, *Ann.Rev.Astron. & Astrphys.*, 32, 277
- Fasano, G., & Vio, R. 1991, *MNRAS*, 249, 629
- Fasano, G., Amico, P., Bertola, F., Vio, R., & Zeilinger, W. W. 1993, *MNRAS*, 262,109
- Fasano, G., et al. 2006, *A&A*, 445, 805
- Fasano, G., et al. 2007, *From Stars to Galaxies: Building the Pieces to Build Up the Universe*, A. Vallenari, R. Tantalo, L. Portinari, & A. Moretti, ASP Conference Series, 374, 495
- Flores, R. A., Allgood, B., Kravtsov, A. V., Primack, J. R., Buote, D. A., & Bullock, J. S. 2007, *MNRAS*, 377, 883
- Franx, M., Illingworth, G., & de Zeeuw, T. 1991, *ApJ*, 383, 112
- Gallagher, J. S. III, & Ostriker, J. P. 1972, *AJ*, 77, 288
- Gao, L., White, S.D.M., Jenkins, A., Stoehr, F., & Springel, V. 2004, *MNRAS*, 355, 819
- Giacintucci, S., Venturi, T., Murgia, M., Dallacasa, D., Athreya, R., Bardelli, S., Mazzotta, P., & Saikia, D. J. 2007, *A&A*, 476, 99
- Gottlöber, S., & Yepes, G. 2007, *ApJ*, 664, 117
- Hashimoto, Y., Henry, J. P., & Boehringer, H. 2008, *MNRAS*, 390, 1562
- Hoessel, J. G., Oegerle, W. R., & Schneider, D. P. 1987, *AJ*, 94, 1111
- Jones, C., & Forman, W. 1984, *ApJ*, 276, 38
- Katayama, H., Hayashida, K., Takahara, F., & Fujita, Y. 2003, *ApJ*, 585, 687
- Kazantzidis, S., Kravtsov, A. V., Zentner, A. R., Allgood, B., Nagai, D., & Moore, B. 2004, *ApJLett*, 611, L73
- Kimm, T., & Yi, S. K. 2007, *ApJ*, 670, 1048
- Kormendy, J., & Djorgovski, S. 1989, *Ann. Rev. Astron. & Astrophys.*, 27, 235
- Laine, S., van der Marel, R. P., Lauer, T. R., Postman, M., O'Dea, C. P., & Owen, F. N. 2003, *AJ*, 125, 478
- Lin, Y., & Mohr, J. J. 2004, *ApJ*, 617, 879
- Lotz, J. M., Primack, J., & Madau, P. 2004, *AJ*, 128, 163
- Loubser, S. I., Sánchez-Blázquez, P., Sansom, A. E., & Soechting, I. K. 2009, *MNRAS*, 398, 133
- Lucy, L. B. 1974, *AJ*, 79, 745
- Macciò, A. V., Dutton, A. A., & van den Bosch, F. C. 2008, *MNRAS* 391, 1940
- Méndez-Abreu, J., Aguerri, J. A. L., Corsini, E. M. & Simonneau, E. 2008, *A&A*, 478, 353
- Merritt, D. 1985, *ApJ*, 289, 18
- Noerdlinger, P. D. 1979, *ApJ*, 234, 802
- Oegerle, W. R., & Hoessel, J. G. 1991, *ApJ*, 375, 15
- Oemler, A. Jr. 1976, *ApJ*, 209, 693
- Ostriker, J. P., & Tremaine, S. D. 1975, *ApJLett.*, 202, 1130
- Patel, P.; Maddox, S., Pearce, F. R., Aragón-Salamanca, A., & Conway, E. 2006, *MNRAS*, 370, 851
- Paturel, G., Petit, C., Prugniel, Ph., Theureau, G., Rousseau, J., Brouty, M., Dubois, P., & Cambrèsy, L. 1993, *A&A*, 412, 45
- Pignatelli, E., Fasano, G., & Cassata, P. 2006, *A&A*, 446, 373
- Plionis, M., Benoist, C., Maurogordato, S., Ferrari, C., & Basilakos, S. 2003, *ApJ*, 594, 144
- Poggianti, B. M., et al. 2009, *ApJLett.*, 697, 137
- Richstone, D. O. 1975, *ApJ*, 200, 535
- Richstone, D. O. 1976, *ApJ*, 204, 642
- Ryden, B. 1992, *ApJ*, 396, 445
- Ryden, B. S., Lauer, T. R., & Postman, M. 1993, *ApJ*, 410, 515
- Sandage, A., & Hardy, E. 1973, *ApJSupp.*, 183, 743
- Schneider, D. P., Gunn, J. E., & Hoessel, J. G. 1983, *ApJ*, 268, 476
- Schombert, J. M. 1986, *ApJSupp*, 60, 603
- Schombert, J. M. 1987, *ApJSupp.*, 64, 643
- Schombert, J. M. 1988, *ApJ*, 328, 475
- Schombert, J. M. 1992, *Morphological and Physical Clas-*

- sification of Galaxies, G. Longo, M. Capaccioli, & G. Busarello, *A&A*, 178, 53
- Silk, J. 1976, *ApJ*, 208, 646
- Stott, J. P., Edge, A. C., Smith, G. P., Swinbank, A. M. & Ebeling, H. 2008, *MNRAS*, 384, 1502
- Struble, M. F. 1990, *AJ*, 99, 743
- Thuan, T. X., & Romanishin, W. 1981, *ApJ*, 248, 439
- Tremblay, B., & Merritt, D. 1996, *AJ*, 111, 2243
- Valentinuzzi, T., et al. 2009, [arXiv:0907.2392]
- Varela, J., et al. 2009, *A&A*, 497, 667
- Vanzella, E., Cristiani, S., Fontana, A., Nonino, M., Arnouts, S., Giallongo, E., Grazian, A., Fasano, G., Popesso, P., Saracco, P., & Zaggia, S. 2004, *A&A*, 423, 761
- von der Linden, A., Best, P. N., Kauffmann, G., White, S. D. M. 2007, *MNRAS*, 379, 867
- Wang, Y., Yang, X., Mo, H. J., Li, C., van den Bosch, F. C., Fan, Z., & Chen, X. 2008, *MNRAS*, 385, 1511
- Warren, M. S., Quinn, P. J., Salmon, J. K., & Zurek, W. H. 1992, *ApJ*, 399, 405
- West, M. J. 1994, *MNRAS*, 268, 79
- Whiley, I. M., et al. 2008, *MNRAS*, 387, 1253
- White, S. D. M. 1976, *MNRAS*, 177, 717

Table 1. Main properties of the BCG sample and of the host clusters

Cluster	$\text{Log}(L_X)^{(a)}$ $10^{44}\text{ergs s}^{-1}$	$\text{Log}(\Sigma)^{(b)}$ km s^{-1}	$z^{(c)}$	WINGS_ID ^(d)	$\text{Ty}^{(e)}$	$M_V^{(f)}$	$M_K^{(g)}$	$R_e^{(h)}$ kpc	$n^{(i)}$	$q_G^{(j)}$	$q_{15}^{(k)}$	$q_{30}^{(l)}$	$q_{60}^{(m)}$	$q_S^{(n)}$	$q_L^{(o)}$
A85	4.28	3.022	0.0551	WINGSJ004150.45-091811.5	cD	-23.89	-26.89	33.86	2.5	0.707	0.770	0.710	0.640	0.610	0.641
A119	1.65	2.936	0.0444	WINGSJ005616.12-011519.0	cD	-23.45	-26.58	25.67	3.6	0.769	0.740	0.690	0.520	0.545	0.767
A133	1.82	2.908	0.0566	WINGSJ010241.72-215255.4	cD	-23.48	-26.52	28.75	3.0	0.666	0.680	0.590	0.550	0.498	0.527
A147	0.28	2.823	0.0447	WINGSJ010812.04+021138.2	E	-22.96	-25.61	26.44	4.4	0.769	0.770	0.770	0.770	0.789	0.776
A151	0.52	2.881	0.0532	WINGSJ010851.13-152423.0	E	-24.08	-26.58	52.03	5.0	0.773	0.800	0.720	0.760	0.789	0.706
A160	0.19	2.749	0.0438	WINGSJ011259.57+152928.8	cD	-22.99	-25.89	26.78	3.7	0.780	0.800	0.720	0.720	0.691	0.716
A168	0.56	2.702	0.0450	WINGSJ011457.58+002551.1	E	-23.16	-26.06	21.47	4.8	0.799	0.800	0.700	0.670	0.620	0.708
A193	0.79	2.880	0.0485	WINGSJ012507.64+084157.2	cD	-24.67	-26.52			0.879	0.880	0.730	0.760	0.752	0.589
A311	0.41		0.0661	WINGSJ020928.41+194636.2	cD	-23.59	-26.94	43.09	4.7	0.576	0.630	0.520	0.460	0.445	0.519
A376	0.71	2.930	0.0476	WINGSJ024603.94+365419.1	cD	-23.55	-26.25	49.09	5.9	0.876	0.890	0.790	0.700	0.693	0.869
A500	0.72	2.818	0.0678	WINGSJ043852.51-220639.0	cD	-23.55	-26.26	44.62	7.0	0.780	0.760	0.620	0.630	0.662	0.664
A548b	0.15	2.928	0.0416	WINGSJ054529.62-255556.8	cD	-21.57		4.88	3.2	1.021	0.940	0.790	0.790	0.847	0.460
A602	0.57	2.857	0.0619	WINGSJ075326.61+292134.4	E	-22.49	-25.14	23.37	3.0	0.832	0.800	0.760	0.760	0.721	0.589
A671	0.45	2.957	0.0507	WINGSJ082831.66+302553.0	cD	-24.04	-26.72	51.55	5.5	0.766	0.790	0.720	0.670	0.675	0.698
A754	4.09	3.000	0.0547	WINGSJ090832.39-093747.3	cD	-23.99	-26.58	47.72	4.5	0.721	0.700	0.730	0.650	0.651	0.776
A780	3.38	2.866	0.0539	WINGSJ091805.68-120543.2	cD	-23.66	-26.04	39.18	4.4	0.838	0.820	0.800	0.730	0.742	0.537
A957	0.40	2.851	0.0451	WINGSJ101338.27-005531.2	E	-23.69	-26.63	28.91	4.3	0.877	0.810	0.790	0.790	0.777	0.710
A970	0.77	2.883	0.0591	WINGSJ101725.71-104120.2	E	-23.18	-25.40			0.856	0.720	0.750	0.780	0.788	0.589
A1069	0.48	2.839	0.0653	WINGSJ103943.44-084112.3	E	-23.62	-26.12	34.87	4.5	0.868	0.760	0.870	0.870	0.875	0.735
A1291	0.22	2.632	0.0509	WINGSJ113223.22+555803.0	cD	-22.79	-25.17	37.33	4.2	0.745	0.840	0.570	0.580	0.513	0.671
A1631a	0.37	2.806	0.0461	WINGSJ125318.41-153203.8	E	-23.35	-26.20	31.15	5.8	0.728	0.740	0.700	0.710	0.689	0.708
A1644	0.04	3.033	0.0467	WINGSJ125711.60-172434.0	cD	-23.94	-25.14	44.93	2.9	0.638	0.630	0.590	0.520	0.525	0.557
A1668	0.81	2.812	0.0634	WINGSJ130346.60+191617.4	E	-23.27	-26.17	26.58	3.2	0.751	0.760	0.730	0.730	0.714	0.895
A1736	1.21	2.931	0.0458	WINGSJ132644.09-272621.8	cD	-23.41	-27.65			0.747	0.670	0.630	0.630	0.620	0.513
A1795	5.67	2.860	0.0633	WINGSJ134852.51+263534.5	cD	-23.89	-26.66	52.00	4.2	0.707	0.760	0.740	0.540	0.531	0.603
A1831	0.97	2.735	0.0634	WINGSJ135915.11+275834.5	cD	-24.49	-27.00	95.06	5.9	0.689	0.730	0.650	0.540	0.572	0.530
A1983	0.24	2.722	0.0447	WINGSJ145255.33+164210.5	E	-22.64	-25.23	27.83	4.5	0.934	0.920	0.910	0.880	0.856	0.955
A1991	0.69	2.777	0.0584	WINGSJ145431.50+183832.8	cD	-23.32	-26.20	30.85	3.1	0.658	0.700	0.640	0.590	0.571	0.641
A2107	0.56	2.772	0.0410	WINGSJ153938.92+214658.1	E	-23.41	-26.43	24.95	3.1	0.787	0.810	0.710	0.710	0.715	0.295
A2124	0.69	2.904	0.0666	WINGSJ154459.02+360633.9	cD	-23.77	-26.77	36.33	3.2	0.737	0.780	0.720	0.650	0.629	0.659
A2149	0.42	2.548	0.0679	WINGSJ160128.11+535650.3	E	-24.29	-26.60			0.788	0.850	0.780	0.760	0.711	0.791
A2169	0.23	2.707	0.0578	WINGSJ161358.09+491122.3	E	-23.25	-25.28			0.741	0.720	0.720	0.660	0.629	0.710
A2256	3.60	3.105	0.0581	WINGSJ170427.22+783825.4	cD	-23.60	-26.44	27.43	3.5	0.866	0.840	0.830	0.850	0.898	0.883
A2271	0.32	2.702	0.0576	WINGSJ171816.66+780106.2	E	-23.75	-26.25	56.14	4.8	0.709	0.760	0.670	0.670	0.634	0.676
A2382	0.46	2.948	0.0641	WINGSJ215155.62-154221.2	E	-23.29	-26.47	35.33	5.1	1.058	0.970	0.920	0.920	0.828	0.513
A2399	0.51	2.852	0.0578	WINGSJ215701.72-075022.0	cD	-22.84	-25.96	13.19	3.2	0.719	0.740	0.780	0.780	0.845	0.746
A2415	0.86	2.843	0.0575	WINGSJ220526.12-054431.1	cD	-22.90	-26.14	20.75	5.2	0.731	0.720	0.620	0.620	0.594	0.592
A2457	0.73	2.763	0.0584	WINGSJ223540.81+012905.8	cD	-23.53	-26.59	36.83	5.2	0.684	0.740	0.590	0.580	0.583	0.662
A2572a	0.52	2.800	0.0390	WINGSJ231711.95+184204.7	E	-21.31	-26.64	3.12	2.5	0.901	0.880	0.510	0.570	0.577	0.849
A2589	0.95	2.912	0.0419	WINGSJ232357.44+164638.3	cD	-23.83	-26.30	61.08	5.1	0.707	0.740	0.570	0.410	0.408	0.501
A2593	0.59	2.846	0.0417	WINGSJ232420.08+143849.8	cD	-23.05	-26.30	21.29	2.8	0.650	0.660	0.620	0.610	0.613	0.635
A2622	0.55	2.843	0.0610	WINGSJ233501.47+272220.9	cD	-23.14	-26.22	24.05	4.2	0.703	0.720	0.650	0.610	0.582	0.646
A2626	0.99	2.796	0.0548	WINGSJ233630.49+210847.3	cD	-23.27	-26.48	25.62	2.3	0.666	0.720	0.670	0.630	0.618	0.723
A2657	0.82	2.581	0.0402	WINGSJ234457.42+091135.2	cD	-22.66	-25.56	32.60	3.5	0.691	0.650	0.630	0.640	0.628	0.631

Table 1. (continue) Main properties of the BCG sample and of the host clusters

Cluster	$\text{Log}(L_X)^{(a)}$ $10^{44} \text{ergs s}^{-1}$	$\text{Log}(\Sigma)^{(b)}$ km s^{-1}	$z^{(c)}$	WINGS_ID ^(d)	Ty ^(e)	$M_V^{(f)}$	$M_K^{(g)}$	$R_e^{(h)}$ kpc	$n^{(i)}$	$q_G^{(j)}$	$q_{15}^{(k)}$	$q_{30}^{(l)}$	$q_{60}^{(m)}$	$q_S^{(n)}$	$q_L^{(o)}$
A2665	0.97		0.0556	WINGSJ235050.55+060858.9	E	-23.59	-26.53	34.02	3.4	0.797	0.830	0.780	0.720	0.742	0.000
A2717	0.52	2.743	0.0490	WINGSJ000312.95-355613.3	cD	-23.56	-26.24	42.48	4.7	0.921	0.870	0.940	0.930	0.932	0.979
A2734	1.30	2.744	0.0625	WINGSJ001121.64-285115.5	cD	-23.44	-26.47	24.66	5.2	0.856	0.760	0.610	0.630	0.513	0.621
A3128	2.71	2.946	0.0600	WINGSJ032950.60-523446.8	cD	-24.18	-26.42			0.928	0.880	0.810	0.780	0.697	0.731
A3158	2.71	3.036	0.0593	WINGSJ034329.69-534131.7	E	-23.41	-26.34	22.37	4.1	0.922	0.920	0.900	0.920	0.888	0.851
A3266	3.14	3.136	0.0593	WINGSJ043113.27-612711.9	cD	-24.51	-27.20	98.44	6.2	0.649	0.700	0.550	0.540	0.548	0.548
A3376	1.27	2.892	0.0461	WINGSJ060041.09-400240.4	cD	-23.32	-26.20	28.11	4.7	0.669	0.670	0.630	0.620	0.599	0.635
A3395	1.43	2.898	0.0500	WINGSJ062736.25-542657.9	cD	-23.29	-26.31	46.78	4.1	0.478	0.470	0.410	0.420	0.447	0.381
A3490	0.88	2.841	0.0688	WINGSJ114520.15-342559.3	cD	-23.72	-26.61	62.34	6.8	0.661	0.590	0.570	0.590	0.540	0.603
A3497	0.74	2.861	0.0680	WINGSJ115946.30-313141.6	E	-22.45	-25.47	13.19	5.5	0.857	0.710	0.730	0.730	0.737	0.755
A3528a	0.68	2.954	0.0535	WINGSJ125441.01-291339.5	cD	-23.77	-27.15	13.08	2.2	0.956	0.990	0.940	0.940	0.910	0.834
A3528b	1.01	2.936	0.0535	WINGSJ125422.23-290046.8	cD	-24.04	-26.74	69.87	6.7	0.695	0.690	0.620	0.620	0.572	0.634
A3530	0.44	2.751	0.0537	WINGSJ125535.99-302051.3	cD	-24.17	-27.07	85.40	5.7	0.713	0.500	0.560	0.620	0.659	0.488
A3532	1.44	2.793	0.0554	WINGSJ125721.97-302149.1	cD	-24.55	-26.60			0.777	0.770	0.690	0.720	0.769	0.000
A3556	0.48	2.747	0.0479	WINGSJ132406.71-314011.6	cD	-23.53	-26.52	27.62	5.2	0.689	0.670	0.790	0.820	0.804	0.594
A3558	3.20	2.961	0.0480	WINGSJ132756.84-312943.9	cD	-23.97	-27.10	34.63	2.8	0.727	0.720	0.670	0.460	0.463	0.618
A3560	0.67	2.851	0.0489	WINGSJ133225.76-330808.9	E	-21.99	-26.07			0.781				0.680	0.000
A3667	4.47	2.997	0.0556	WINGSJ201227.32-564936.3	cD	-23.98	-26.69	41.44	4.0	0.914	0.950	0.790	0.620	0.572	0.689
A3716	0.52	2.921	0.0462	WINGSJ205156.94-523746.8	cD	-23.77	-26.80	32.60	4.2	0.739	0.740	0.660	0.640	0.642	0.525
A3809	1.15	2.751	0.0627	WINGSJ214659.07-435356.2	E	-23.11	-25.82	23.13	3.2	0.782	0.830	0.710	0.730	0.720	0.783
A3880	0.95	2.883	0.0584	WINGSJ222754.43-303431.8	cD	-23.18	-26.51	20.22	2.6	0.889	0.880	0.740	0.710	0.609	0.793
A4059	1.58	2.854	0.0475	WINGSJ235700.71-344532.8	cD	-23.95	-26.87	38.99	3.0	0.676	0.680	0.620	0.580	0.506	0.600
IIZW108	1.12	2.710	0.0483	WINGSJ211355.90+023355.4	cD	-23.78		46.30	2.8	0.627	0.690	0.620	0.510	0.527	0.543
MKW3s	1.37	2.732	0.0444	WINGSJ152151.84+074232.1	cD	-23.36	-25.61	48.87	5.9	0.691	0.600	0.590	0.590	0.557	0.548
RXJ0058	0.22	2.804	0.0484	WINGSJ005822.88+265152.6	cD	-23.78		47.13	5.4	1.013	0.830	0.970	0.890	0.898	0.000
RXJ1022	0.18	2.761	0.0548	WINGSJ102237.40+383445.0	E	-22.33	-25.81	20.23	4.4	0.724	0.740	0.620	0.650	0.634	0.578
RXJ1740	0.26	2.765	0.0441	WINGSJ174032.06+353846.1	cD	-22.75	-25.78	22.33	3.4	0.627	0.660	0.530	0.510	0.502	0.000
ZwCl1261	0.41		0.0644	WINGSJ071641.24+532309.4	cD	-23.78	-27.08	43.48	4.8	0.711	0.730	0.610	0.480	0.530	0.000
ZwCl2844	0.29	2.729	0.0503	WINGSJ100236.54+324224.3	cD	-23.21	-26.26	19.15	4.3	0.755	0.760	0.510	0.390	0.384	0.537
ZwCl8338	0.40	2.852	0.0494	WINGSJ181105.18+495433.7	cD	-23.54	-26.59	25.45	4.9	0.845	0.840	0.800	0.810	0.801	0.692
ZwCl8852	0.48	2.884	0.0408	WINGSJ231042.27+073403.7	E	-23.26	-26.44	17.39	4.9	0.911	0.880	0.900	0.890	0.862	0.891

(a) Decimal logarithm of the X-ray luminosities in the 0.1-2.4 keV band from Ebeling et al. (1996, 1998, 2000)

(b)-(c) Decimal logarithm of the velocity dispersions of cluster galaxies (b) and average redshifts of clusters (c) from Cava et al. (2009). Some values have been updated, according to Cava et al. (2010).

(d) WINGS identifier from Varela et al. (2009).

(e) Morphological type (see text).

(f) Total absolute magnitude in the V-band from Varela et al. (2009, corrected for galactic extinction)

(g) Total absolute magnitude in the K-band from 2MASS.

(h) Effective radius in kpc from GASPHOT. Missing values indicate that GASPHOT failed to converge.

(i) Sersic index from GASPHOT. Missing values indicate that GASPHOT failed to converge.

(j) Axial ratio at the effective isophote from GASPHOT. In case GASPHOT failed to converge, we derive q_G from the equation: $q_G=0.392+0.572 \times q_S$ (obtained from the linear best-fitting of the relation in panel 15 of Figure 1).

(k)-(m) Axial ratios of the isophotes at 15, 30 and 60 kpc of major axis [(k), (l) and (m), respectively] from GASPHOT.

(n) Axial ratio at the threshold area from Varela et al. (2009, SExtractor).

(o) Axial ratio from the LEDA Hypercat database (Paturel et al. 2003).

Table 2. Main properties of the additional cD sample

Cluster	WINGS_ID	rank ^(a)	M_V	M_K kpc	R_e	n	q_G	q_{15}	q_{30}	q_{60}	q_S	q_L
A548b	WINGSJ054527.59-255550.9	3	-22.17	-25.00			0.740	0.750	0.790	0.790	0.608	0.000
A602	WINGSJ075316.63+292405.3	2	-21.87	-25.07			0.724	0.660	0.590	0.600	0.580	0.000
A1736	WINGSJ132727.99-271929.2	2	-23.76	-26.65	31.33	5.2	0.607	0.620	0.510	0.570	0.614	0.542
A1736	WINGSJ132800.12-272115.5	3	-23.15	-26.48			0.854	0.730	0.760	0.760	0.808	0.724
A1831	WINGSJ135908.75+280121.3	2	-23.36	-26.29			0.594	0.480	0.410	0.370	0.353	0.000
A1983	WINGSJ145243.26+165413.5	2	-22.54	-25.55	9.47	4.5	0.693	0.660	0.600	0.600	0.588	0.689
A3158	WINGSJ034252.97-533752.6	3	-22.64	-26.60	12.78	4.3	0.826	0.830	0.650		0.762	0.525
A3266	WINGSJ043021.97-613200.7	2	-22.87	-26.12			0.886	0.880	0.900	0.890	0.863	0.000
A3395	WINGSJ062649.57-543234.5	2	-24.09	-26.03			0.975	0.930	0.910	0.920	0.835	0.813
A3528a	WINGSJ125452.41-291617.1	2	-22.30	-25.77			0.711	0.550	0.550	0.550	0.557	0.000
A3556	WINGSJ132329.02-315039.6	2	-24.41	-26.34			0.877	0.830	0.710	0.670	0.661	0.631
ZwC18338	WINGSJ181109.74+495153.0	2	-22.47	-25.70			0.712	0.640	0.620	0.580	0.560	0.000
ZwC18852	WINGSJ231022.37+073450.5	2	-22.84	-26.19	14.58	2.8	0.683	0.620	0.560	0.550	0.509	0.558
ZwC18852	WINGSJ231030.43+073520.6	3	-22.89	-25.88			0.760	0.830	0.690	0.700	0.644	1.000

(a) Luminosity ranking in the V-band

APPENDIX A: DISENTANGLING CDS FROM BCG_ES WITH MORPHOT

MORPHOT is an automatic tool for galaxy morphology, puposely devised in the framework of the WINGS project. An exhaustive description of the tool will be given in a forthcoming paper (Fasano et al., in preparation). Here we just outline the logical sequence and the basic procedures of MORPHOT. It extends the classical CAS (Concentration/Asymmetry/clumpiness) parameter set (Conselice 2003), by using 20 image-based morphological diagnostics. Fourteen of them have never been used, while the remaining six are actually already present in the literature, although in slightly different forms: the Sersic index, the Concentration index (Conselice 2003), the Gini and M20 coefficients (Lotz et al. 2004), the Asymmetry and Clumpiness parameters (Conselice 2003).

Besides depending on the visual morphology, all diagnostic are also empirically found to depend on the relative size (area enclosing 80% of the total light divided by FWHM area) and flattening of galaxies, as well as on the image S/N ratio. These ‘a priori’ dependencies have been removed using a sizeable set of simulated galaxies and a control sample of ~ 1500 WINGS+SDSS galaxies, visually classified by two of us (GF and AD). These visual classifications have been used to calibrate and combine the 20 diagnostics, thus obtaining a final, single estimator of the morphological type, equipped with the proper confidence interval. This has been achieved by averaging the results of two different, totally independent approaches, based on the Neural Network (NN) and Maximum Likelihood (ML) techniques. The first approach (NN) is based on a particular kind of feed-forward Neural Network, called Multilayer Perceptron Artificial NN (MLP, see Vanzella et al. 2004). In this case the control galaxy sample provides the training set of the NN machine, with the morphological diagnostics used as inputs and the visual classifications as targets. In the ML-based approach the probability density distributions of all diagnostics for all morphological types are drawn from the control galaxy sample. In this case the ‘blind’ morphological type estimate of any other galaxy is obtained maximizing the product of the probabilities of the particular set of diagnostics derived from the galaxy image.

Defining each diagnostic and explaining its meaning is beyond the scope of the present paper. Here we just mention that all diagnostics are normalized to vary in the range (0–1) and that four out of the 14 newly devised diagnostics turned out to be the most effective ones in order to disentangle cDs from BCG_Es. They are: (i) a modified version of the Gini coefficient (*GID*), where the pixels are sorted according to the distance from the galaxy center, rather than according to the flux (as in Lotz et al. 2004); (ii) a Diskiness coefficient (*DSK*), measuring the correlation between azimuth and pixel flux relative to the average flux value of the elliptical isophote passing through the pixel itself; (iii) an image-averaged 2D-Laplacian (*LAP*) in polar coordinates, roughly quantifying the global degree of concaveness of the galaxy profile; (iv) an Alignment coefficient (*ALI*), measuring the average concordance between the (local) maximum flux gradient direction and the (local) direction of the galaxy center.

In Figure A1, the cumulative distributions of the four

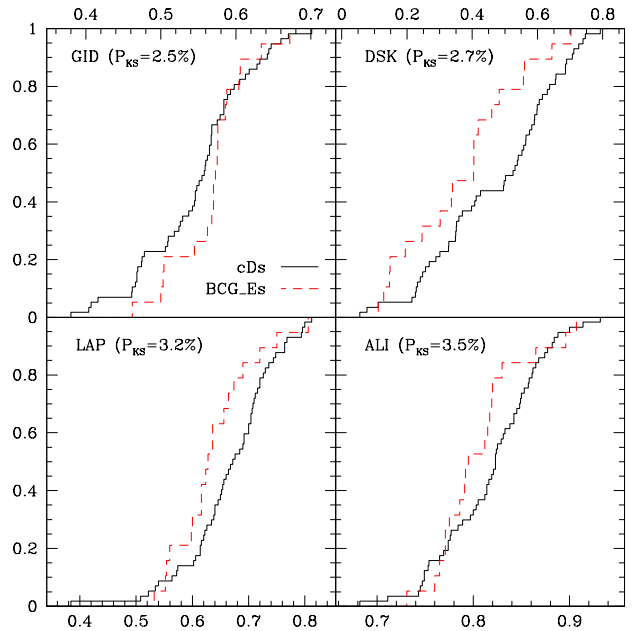


Figure A1. Comparison between cDs (full line) and BCG_Es (dashed line; red in the electronic version) for the cumulative distributions of the morphological diagnostics *GID*, *DSK*, *LAP* and *ALI* (see text for a short description of them).

above mentioned diagnostics for cDs and BCG_Es are reported for comparison, together with the relative KS probabilities. The figure shows that, compared with BCG_Es, the cD galaxies have (on average) lower values of *GID* (less peaked profiles) and larger values of *DSK* (more diskly), *LAP* (more concave) and *ALI* (local gradient better aligned with the galaxy center). Even if none of the four diagnostics illustrated in the figure, alone, turns out to be conclusive, their combination (through MORPHOT) provides us with a powerful tool for the particular task of disentangling cDs from BCG_Es.